INVESTIGATION OF HEAT TRANSFER AND BONDING DURING MATERIAL JETTING ADDITIVE MANUFACTURING

by

Krishna Khanal

A thesis submitted to Graduate Faculty of

Auburn University

in partial fulfillment of the

requirements for the Degree of

Master of Science

Auburn, Alabama

December 15, 2018

Keywords: additive manufacturing, deposition, interfacial bond, interfacial heat transfer coefficient

Approved by

Ruel A. Overfelt, Chair, Professor of Material Engineering

Roy W. Knight, Associate Professor of Mechanical Engineering

Daniel Mackowski, Professor of Mechanical Engineering

Abstract

Optimum process parameters are critical to achieve deposits of high metallurgical integrity during material jetting additive manufacturing. The most important process parameters include deposition temperature, substrate temperature, mass deposition rate, velocity of material jetting and the level of oxygen. This document describes experiments and analyses to determine these parameters using pure tin as a model deposition material. Molten tin at 400^0C was deposited through a 250μm diameter nozzle at a velocity of 1m/s onto a tin substrate maintained at either 150^0C, 175^0C or 195^0C. The deposition experiments were carried out under ambient air and inert gas (N_2) environments. The experimental results showed that better metallurgical bonding was obtained at 195^0C substrate temperature in N_2 gas environment and these parameters also gave consistent results during shear tests.

A simple heat transfer model is presented to describe the heat flow from a deposition to the substrate. Hypothesized Newtonian cooling agreed with the experimental temperature results which enabled experimental determination of the interfacial heat transfer coefficient h_i. In addition 2-D axisymmetric transient numerical simulations have been carried out using the empirical h_i data and the results agreed with experiments. This work demonstrated use of appropriate process parameters to get good metallurgical bonding.

Acknowledgements

I would like to thank my advisor, Dr. Ruel A. Overfelt, for giving me the opportunity to work in this research and for the guidance during the entire research. I would also like to show my gratitude towards the committee members, Dr. Roy Knight and Dr. Daniel Mackowski, for their support. I am very much thankful to Mr. Mike Crumpler for his support in the lab. I would also like to thank Dr. Bart Prorok, Dr. Jordan Roberts and Mr. Steve Moore for their help during the research. Finally, I would like to thank all my friends, family and all other people who directly or indirectly helped me during this research.

Table of Contents

List of Figures

List of Tables

Nomenclature

AM	Additive Manufacturing
ASTM	American Society for Testing and Materials
BJ	Binder Jetting
CNC	Computer Numerical Control
DAQ	Data Acquisition
DED	Direct Energy Deposition
GE	General Electric
IR	Infrared Camera
ISO	International Organization for Standardization
MJ	Material Jetting
NI	National Instruments
PBF	Powder Bed Fusion
SL	Sheet Lamination
VOF	Volume of Fluid
VP	Vat Photo-polymerization
3D	Three Dimensional
1D	One Dimensional
Sn	tin
CFD	Computational fluid dynamics
N_2	Nitrogen gas
ppm	Parts per million
$q_a(n)$	Fourier constants

$q_b(n)$	Fourier constants
w_0	Periodic frequency
h_i	Interfacial heat transfer coefficient ($W/m^2.K$)
f	Frequency (Hz)
d_0	Droplet diameter (m)
T_d	Incoming droplet temperature (^0C)
T_m	Melting point temperature (^0C)
T_b	Base Temperature (^0C)
h_c	Height of column (m)
$R_{t,c}$	Thermal contact resistance at substrate ($m^2.K/W$)
R_f	Thermal resistance of column ($m^2.K/W$)
q	Heat flux (W/m^2)
A_c	Average cross-section area (m^2)
k	Thermal conductivity (W/m.K)
ρ	Density (Kg/m^3)
C_p	Specific heat capacity (J/Kg. K
L_f	Latent heat of fusion (J/Kg)
T	Temperature (^0C)
t	Time (s)
α	Thermal diffusivity (m^2/s)
T_{sub}	Substrate temperature (^0C)
q_0	Average heat flux (W/m^2)
q_A	Amplitude of heat flux (W/m^2)

$q(t)$	Periodic surface heat flux (W/m^2)
t_p	Pulse width (s)
t_0	Time interval between consecutive droplets (s)
V_0	Initial velocity (m/s)
T_0	Initial temperature (^0C)
N_2	Nitrogen gas
ppm	Parts per million
A	Convective surface area of object (m^2)
V	Volume of object (m^3)
T_a	Substrate temperature (^0C)

Chapter 1: Introduction

Additive manufacturing (AM), which is also known as 3D printing, is one of the most evolving manufacturing processes in the modern day world. This method aims to create a complicated product with fewer parts which through other manufacturing means could take more time, effort and cost. The concept of AM is to build a 3D object by adding layer upon layer of material where the material can be plastic, metal, concrete or any potential composite. AM provides greater flexibility than the traditional manufacturing processes like casting and machining. One of the leading manufacturers, General Electric (GE), has been using 3D printing techniques to make jet parts [1]. It has chosen additive manufacturing to generate nozzles of jets by reducing the material consumption and hence decreasing the production cost.

According to the International Organization for Standardization (ISO)/ American Society for Testing and Materials (ASTM) 52900:2015, AM is divided into seven categories [2]: binder jetting (BJ), direct energy deposition (DED), material extrusion (ME), material jetting (MJ), powder bed fusion (PBF), sheet lamination (SL) and vat photo-polymerization (VP). All of these AM processes include a material layer deposited or directed while it is in fluidic state. This research work resides under the category of material jetting additive manufacturing.

1.1 Material Jetting Additive Manufacturing

In this method, material is deposited from the nozzle which moves across the build platform on the build surface layer by layer to make an object. The energy is carried by the material itself to melt the previous deposition and to form a good bond with it. There are two types of material jetting processes: continuous deposition and drop on demand deposition as shown in Figure 1 and Figure 2 respectively.

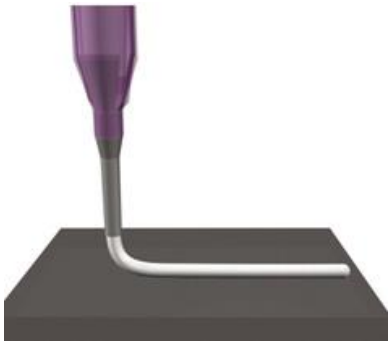

Figure 1: Continuous Deposition

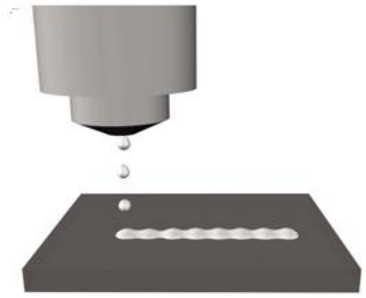

Figure 2: Drop on Demand Deposition

In continuous deposition, material is deposited continuously from nozzle on the build surface while on drop on demand (DoD) deposition material is deposited in the form of drops and sometimes these drops are charged to deflect to the desired location. This research work falls between these two types i.e. material is jetted on continuous manner only for short time which eventually forms drop like shape on the build surface.

Temperature of the material during the process plays a very important role to determine physical characteristic of the product developed. Materials with lower melting points like polymers can be easily cured and bonded upon cooling while it is not easy for higher melting point materials like ceramics and metals. This research is carried out using tin (Sn), which has relatively low melting point than other metals, to investigate the influence of process parameters like deposition temperature, substrate temperature and atmosphere on integrity of bond formation and interfacial

heat transfer coefficient h_i. This research work aims to provide process window to build complex shape objects.

1.2 Objectives

The objectives of this investigation were:

- How process parameters influence:
    - Interfacial bonding in Sn
    - Interfacial heat transfer coefficient h_i during Sn deposition
- Experimentally identify process window to produce more complex shapes
- Demonstrate usage of estimated h_i in Fluent numerical model to predict needed process parameters for more complex shapes

Chapter 2: Literature Review

Several researches have been carried out in the field of AM to understand the principle and process governing this manufacturing technique. Fang et al. [3] presented simple energy balance equation to predict the combination of process parameters on uniform bonding of deposition as the column is built up. Figure 3 shows the 1D model for droplet deposition on vertical column. Here droplets of diameter d_0 having temperature T_d at a frequency f are deposited on a substrate maintained at a temperature T_b to build column of height h_c. Since the formulation is assumed to be 1D without convection and radiation heat loss, energy from droplet has to be carried out by the column. Tip of the growing column is maintained at the melting point temperature T_m to have a good bond with the incoming droplet. Rate of energy carried by droplet is given by Equation (1) and this is transferred by the column which is given by Equation (2). Balancing and rearranging Equation (1) and Equation (2), frequency f can be determined which depends on other process parameters like height of column, droplet temperature, substrate temperature and so on. From Equation (3), it is shown that the frequency of droplet deposition rate should be decreased as height of column rises to maintain tip temperature at melting point. Figure 4 shows the variation of frequency with column height.

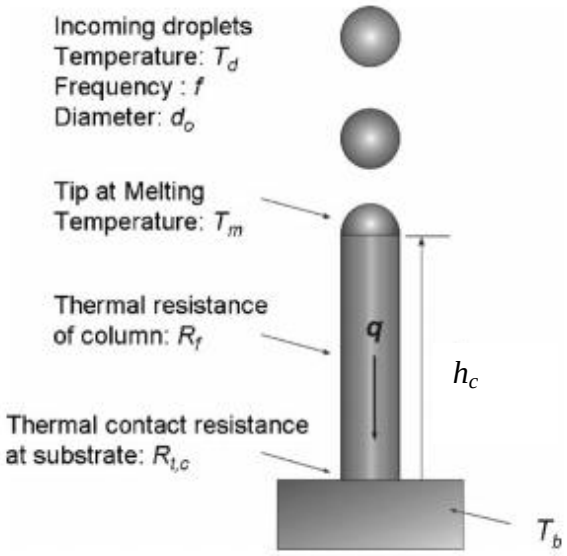

Figure 3: 1D Model for droplet deposition on vertical column [3]

$$\dot{E}_{drop} = f \times \frac{\rho \pi d_0^3}{6} [C_p(T_d - T_m) + L_f] \tag{1}$$

$$\dot{E}_{cond} = \frac{(T_m - T_b)}{\left(R_{t,c} + \frac{h_c}{k}\right)} \times A_c \tag{2}$$

$$f = \frac{6kA_c(T_m - T_b)}{\left(R_{t,c}k + h_c\right)\rho \pi d_0^3 [C_p(T_d - T_m) + L_f]} \tag{3}$$

where, k is thermal conductivity, A_c is average cross-section area of column, $R_{t,c}$ is thermal contact resistance at substrate, is height of column, ρ is density, C_p is specific heat capacity and L is latent heat of the material.

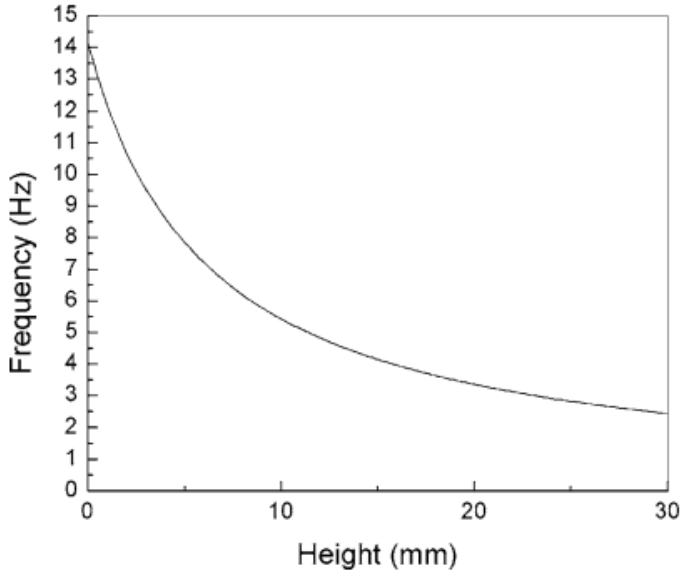

Figure 4: Variation of frequency with column height to maintain tip temperature [2]

Since Equation (2) assumes linear temperature distribution along vertical column, another article by Fang et al. [4] considered droplet deposition as periodic heat flux and solved Fourier heat conduction equation with initial and boundary conditions as given by Equation (5) and Equation (6) respectively. Figure 5 shows the heat transfer model where the periodic series of heat flux is approximated by Fourier series as given by Equation (7) and the conduction problem is solved to get Equation (8) by considering 1D heat transfer problem with no interfacial thermal contact resistant. Figure 6 shows the comparison of experimentally measured and predicted base temperature obtained from Equation (8). This solution is based on constant droplet frequency, however if we have variable frequency the problem becomes very difficult to reach an analytical solution.

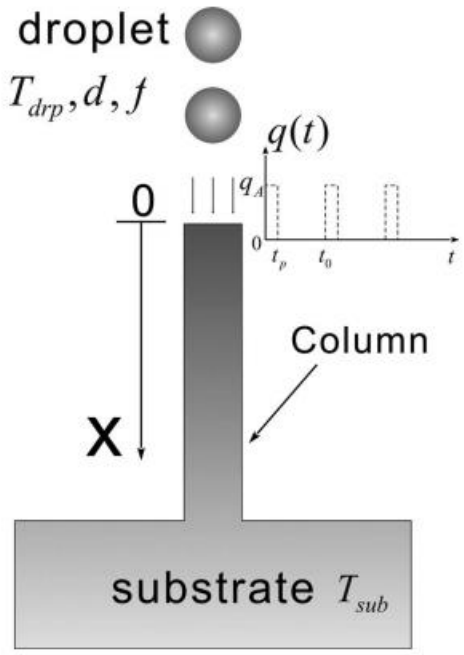

Figure 5: Heat Transfer model [4]

$$\text{Fourier conduction eqn: } \frac{\partial T(x,t)}{\partial t} = \alpha \frac{\partial^2 T(x,t)}{\partial^2 t}, \qquad 0 \le x \le \infty \tag{4}$$

$$\text{Initial Condition: } T(x,0) = T_{sub}, \ t = 0 \tag{5}$$

$$\text{Boundary Condition: } T(\infty,t) = T_{sub}, \ x = \infty \tag{6}$$

$$q(t) = q_o + \sum_{n=1}^{\infty} q_a(n)\cos(nw_0 t) + \sum_{n=1}^{\infty} q_b(n) sin(nw_0 t) \tag{7}$$

$$T(x,t) = T_{sub} + \frac{2q_0}{k}\left(\sqrt{\frac{\alpha t}{\pi}} e^{-x^2/4\alpha t} - \frac{x}{2} erfc\left(\frac{x}{2\sqrt{\alpha t}}\right)\right)$$

$$+ \sum_{n=1}^{\infty} \frac{q_a(n)}{k} \sqrt{\frac{\alpha}{nw_0}} e^{-x\sqrt{nw/2\alpha}} cos\left(nw_0 t - x\sqrt{\frac{nw_0}{2\alpha}} - \frac{\pi}{4}\right) \tag{8}$$

$$+ \sum_{n=1}^{\infty} \frac{q_b(n)}{k} \sqrt{\frac{\alpha}{nw_0}} e^{-x\sqrt{nw/2\alpha}} sin\left(nw_0 t - x\sqrt{\frac{nw_0}{2\alpha}} - \frac{\pi}{4}\right)$$

where, q(t) is periodic surface heat flux, q_A is amplitude of heat flux, $t_p$is pulse width, t_0 is time interval between consecutive droplets, T_{sub} is substrate temperature, q_a and q_b are constant of Fourier series and $w_0 = 2\pi/t_0$.

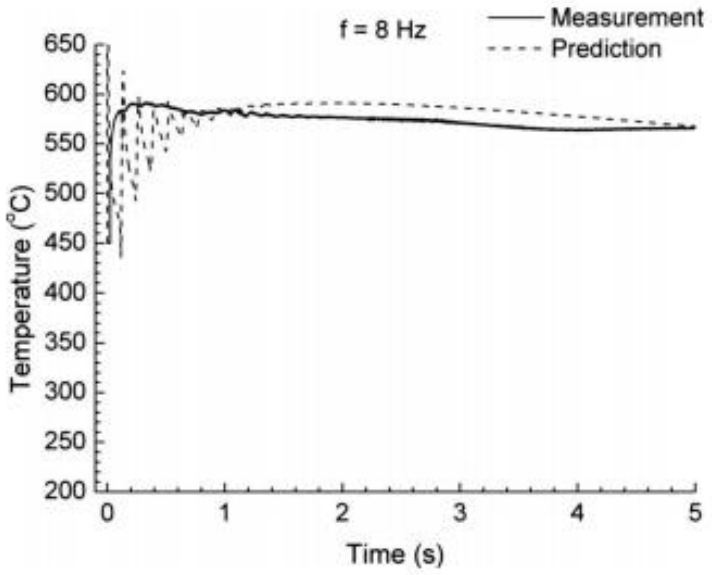

Figure 6: Measured and predicted base temperature during fabrication of column on substrate temperature 450^0C and 8 Hz deposition rate [4]

If single droplet is considered to be deposited on the substrate with assumption of single droplet acting as point source with no thermal resistance between droplet and substrate, then the conductive problem would reduce to instantaneous point source of heat which solution is presented by Carslaw and Jaeger [5] .

Similarly, Chao et al. [6] used 1D analytical model of Fang et al. [3] and found out optimum droplet temperature and base temperature to build certain column height for 1D case. Using this parameter they carried out experiments as well as 3D numerical simulation and showed that 1D heat transfer analytical model also holds good for 3D case which was justified by their

experimental results. 3D numerical model and experimental result is shown in Figure 7 and Figure 8 respectively. Case ‘c’ of experimental result (as shown in Figure 8) has no voids between depositions and has the perfect bonding without distorted geometry.

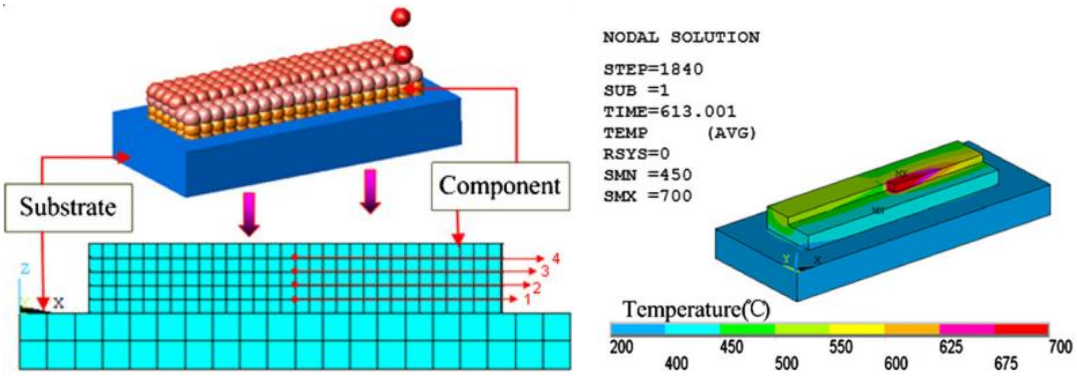

Figure 7: 3D finite element model (left) and temperature contour (right) [6]

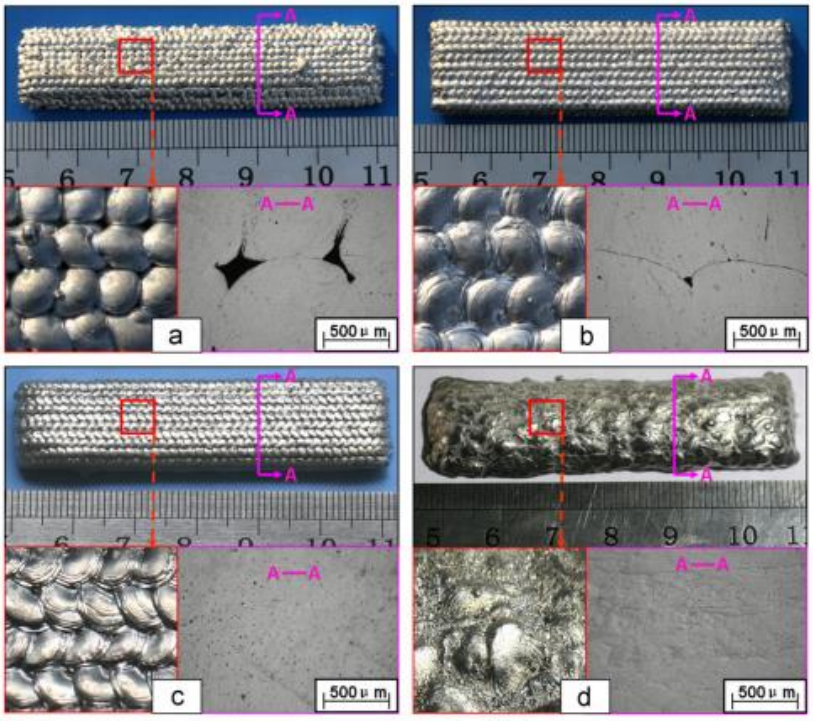

Figure 8: Experimental result for different base and droplet temperature [6]

Kim [7] has presented an analytical solution to heat conduction for moving heat source using Fourier series procedure and compared with numerical results but no experimental validation was provided. Likewise, Elsen et al. [8] has shown the solutions for modeling moving heat sources and its application to laser material processing. They have discussed application and limitation of solutions for different heat source geometry like moving point source, semi-ellipsoidal moving heat source and uniform moving heat source.

Several numerical models have been proposed to study droplet deposition by different researchers. Most investigation was done assuming droplets impact on flat surface by neglecting shrinkage effect due to discrepancy on density of liquid and solid. Li et al. [9] presented 3D numerical simulation of successive deposition on moving substrate by taking into account the fluid dynamics of droplet when impacting and spreading. Figure 9 shows the schematic representation of model for successive droplets deposition and Figure 10 shows temperature distribution after third droplet deposition. Likewise to account the droplet impact on non-flat surface considering fluid dynamics of droplet, Du and Wei [10] numerically investigated pileup process in micro-droplet deposition considering the shrinkage effect and real boundary condition. They were successful to show the numerical and experimental results in agreement. Figure 11 shows boundary and computational domain whereas Figure 12 shows SEM and simulation results for droplet pileup.

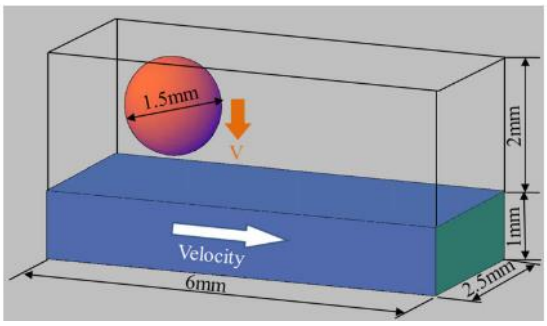

Figure 9: Schematic representation of model for successive droplets deposition [9]

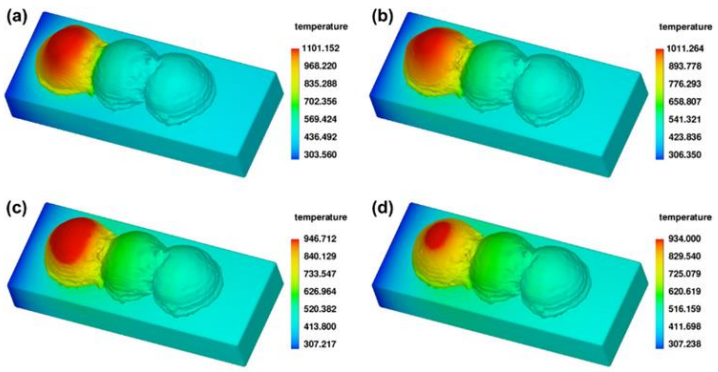

Figure 10: Calculated 3D image with temperature of third droplet after deposition (a) 3 ms (b) 6 ms (c) 9 ms and (d) 12 ms [9]

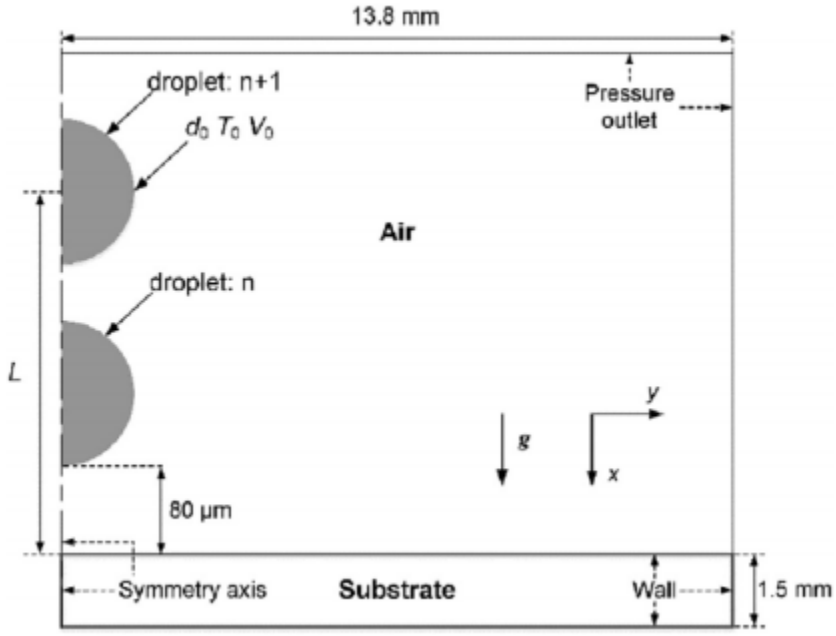

Figure 11: Boundary condition and computational domain [10]

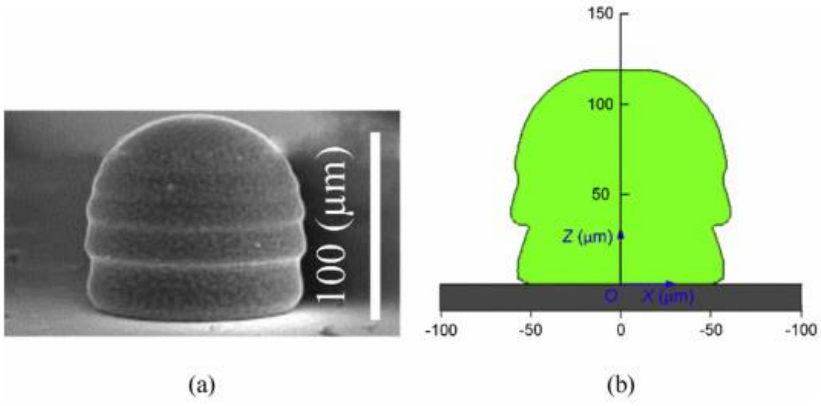

Figure 12: (a) SEM and (b) simulation result for droplet pipeup [10]

Inverse modeling [11] approach of layer by layer liquid metal deposition has been presented to model heat transfer that occurs during layer by layer fabrication which the authors said to be adaptable for prediction of temperature histories within parts of complex geometries. However, this inverse modeling lacks the study of sensitivity and general dependence of temperature histories on changes in boundary conditions and process parameters.

Webb et al. [12] studied the factors affecting successful welded joint formation for a given droplet material and target which would provide the basis for computer modeling to enable rapid process set-up on a production line. They identified parameters for good adhesion of a droplet to a target which are characterized by droplet temperature and target thickness for each material/target droplet combination. Similarly, research by Dhiman and Chandra [13] studied the impact of molten tin droplets (0.6 mm diameter) on solid surfaces for a range of impact velocities (10-30 m/s), substrate temperatures (25-200 ^{0}C) and substrate materials (stainless steel, aluminum and glass). Zuo et al. [14] studied influence of interfacial bonding between metal droplets of aluminum on tensile properties. They showed that with proper temperature setting micro metal deposition could achieve as good mechanical properties as extruded sample.

Some of the research on material jetting is related to droplet generation. One method is pinch-off mechanism from non-wettable nozzle while the other from wettable nozzle. Chang et al. [15] investigated the behaviors of droplet from wettable nozzle by changing nozzle size and fluid flow rate . The behavior of droplet is described by the equation consisting capillary force, viscous drag and gravity. Another article by Yang and Liburdy [16] has described the formation of micro-droplets from vibrating micro-nozzle by a pressure pulse wave. They did numerical investigation considering 1D model and showed that the vibration of nozzle does not influence break off time, however, it affects the droplet volume, shape and satellite droplets. Later, 2D axisymmetric model to study mechanism of droplet formation was proposed by Luo et al. [17] and the results were verified with experimental ones. Impact driven micro-droplets on demand using metal ring connected rod with a solid impactor to create pulse was studied by Luo et al. [18] and showed its benefit over spring type pulse transfer.

Several research studies from droplet generation methods to deposition bond as well as heat transfer model have been proposed and validated using experimental and numerical methods. However, use of Newton's cooling law as heat transfer model in metal deposition has not been carried out, so implementing this model would be a novel approach. Along with this, quantification of bonding due to change in process parameters also needed to be explored. So, this research is carried out to model the material jetting additive manufacturing process to investigate bond formation as well as the heat transfer involved during the process.

Chapter 3: Experimental Setup and Methodology

In this section, experimental setup and methodology of the research is being discussed. Deposition was made on different substrate temperatures on air and inert (N_2) gas. The bonding of deposition to the substrate has been analyzed and relative strength of different cases has been compared. Furthermore, cooling rate of deposition is recorded by thermocouple and fitted with Newton's law of cooling equation to find out the interfacial heat transfer coefficient h_i. Numerical simulations are carried out using the estimated h_i and temperature results are compared with experimental ones.

3.1 Material Selection

To do the experiment, tin material (99.9% pure) was selected for this study because it has a low and a definite melting point (232^0C) which makes it relatively easy for conducting experiments as well as the analysis part. Since the experiment is modeled to be additive manufacturing process, tin is used as both a deposition and a substrate as shown in Figure 13.

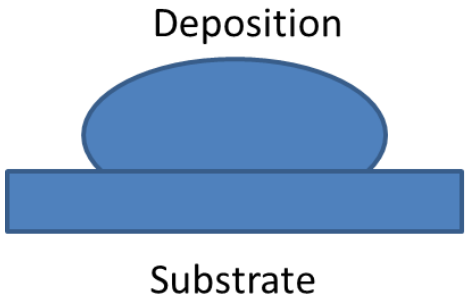

Figure 13: Deposition and Substrate

3.2 Experimental Setup

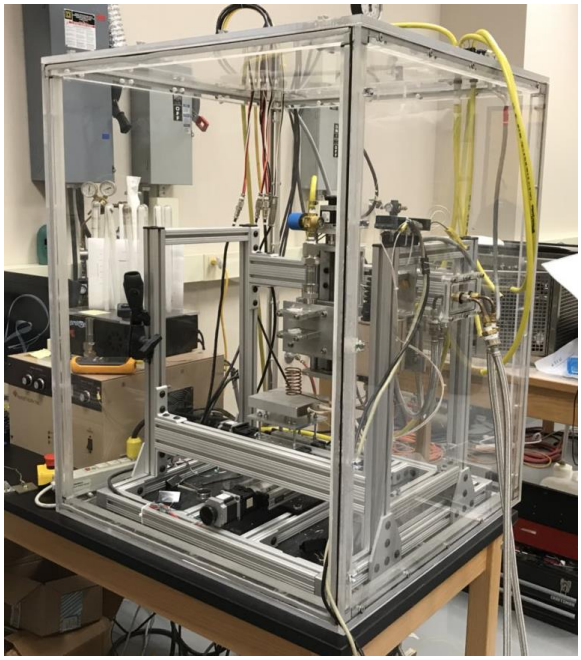

Figure 14: Experimental setup

Figure 14 shows the experimental setup inside a plexi-glass chamber. The CNC machine is enclosed inside a glass chamber and the base plate of CNC can move along the x and y-direction while the nozzle can move along the z-direction. Figure 15 shows the different constituents of experimental setup. Tin material inside the ceramic is heated by induction coil maintained at 110 V with an induction frequency of 127 kHz. Cool water through the induction coil is circulated to stop overheating of the coil. The induction coil generates rapidly changing magnetic field which produces eddy current that heats the material and melts it. A thermocouple is used to measure the temperature of melted tin, which reaches to a steady state of 400^0C at this operating condition (110 V). The pressurizing hose on the top of ceramic tube was fitted to provide a pressure pulse of 6 psi which would eject molten tin from bottom of ceramic tube having a nozzle diameter of 250µm at a velocity of 1m/s (measured by high speed camera). The pressure pulse would last for 0.5 seconds and it was automatically controlled by a computer (Mach 4 software) which helps to

provide constant mass deposition. Experiment was performed both in air as well as in inert gas (N_2) environment with three different substrate temperatures (150^0C, 175^0C, 195^0C). For Inert gas, air was flushed out until the oxygen level was less than 150 ppm which was measured by InterPurge Model 772. The sample image of depositions on tin substrate is shown in Figure 16.

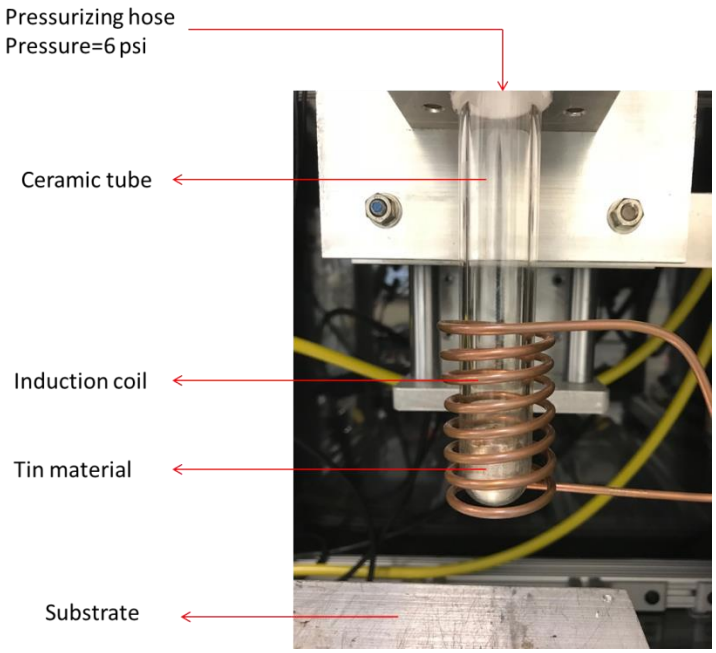

Figure 15: Different parts of experimental setup

Figure 16: Uniform mass deposition on tin substrate

3.3 Sample preparation

Depositions were made on three different substrate temperatures (three cases) in air and N_2 gas. For each case, three samples were prepared for polishing and shear testing. Table 1 summarizes the number of samples for each case. Total number for polishing was 18 which was the same number was for shear test samples.

Table 1: Sample Table

Substrate Temperature (^{0}C)	**Medium**	**Polishing samples number**	**Shear test samples number**
150	Air	3	3
175	Air	3	3
195	Air	3	3
150	N_2	3	3
175	N_2	3	3
195	N_2	3	3
	Total samples	**18**	**18**

3.4 Polishing

For polishing, deposition samples were cut in size of 10 mm by 10 mm including both deposition and substrate to observe interfacial bond. Cut samples were then embedded on a mixture of epoxy and hardener. The samples were polished using silicon carbide grits of 120, 400, 800, 1000 and 1200 and final polishing was made by soft cloth with alumina powder paste of size

0.3µm. After that the interface of deposition and substrate was observed in an Olympus Bx51 microscope and the image was taken to quantify bond length using AutoCAD. Figure 17 shows the polished samples for all cases.

Figure 17: Polished samples

3.5 Shear Test

For shear testing, a fixture to hold deposited material and substrate was designed and made using shop equipment in Wilmore lab. Instron tensile machine of capacity 5000 N was used for shear testing. Figure 18 shows the fixture that held sample were fitted on the tensile machine and a tubular plastic was used as shown in Figure 19 to maintain alignment during the experiment.

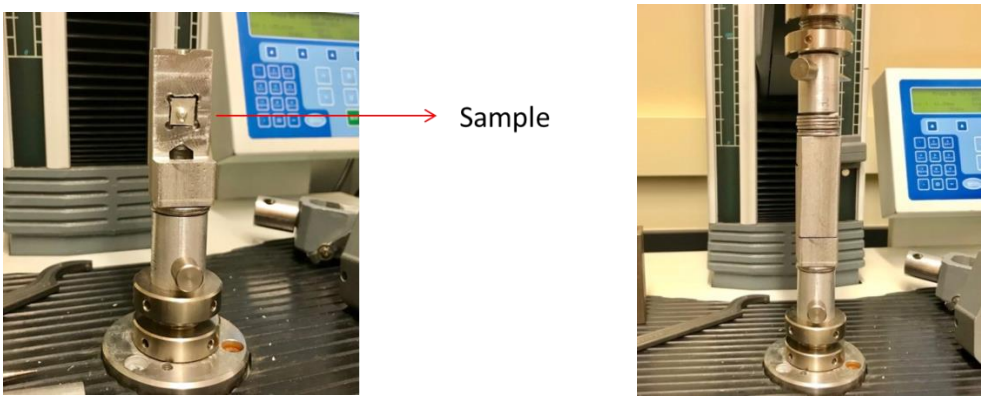

Figure 18: Fixture to hold sample fitted on tensile machine

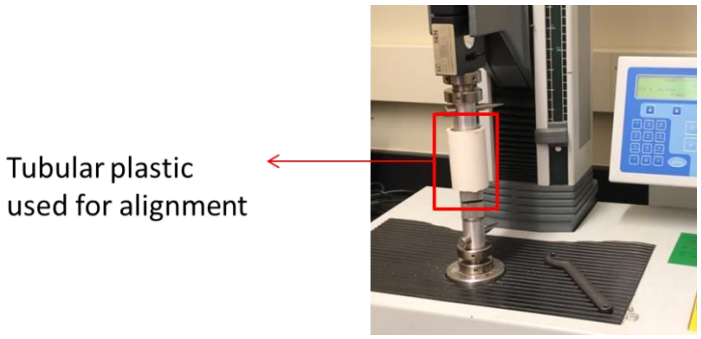

Figure 19: Tubular plastic to make good alignment

3.6 Heat Transfer Model: Newtonian cooling

Newtonian cooling [19] involves the cooling of a lumped mass loosing heat to another body which is maintained at a constant temperature. In this research study, heat transfer from the deposited mass to the substrate was assumed to be dominated by conduction from the deposit to the underlying substrate. Conductive mode of heat transfer from the deposition to the substrate is governed by the heat transfer across the interface between the deposit and the substrate and can be represented by an interfacial heat transfer coefficient, h_i. Now, by assuming substrate as a heat sink the Newtonian cooling approach can be used to model the heat transfer and to estimate the interfacial heat transfer coefficient h_i. Figure 20 shows the Newtonian cooling model and Equations (9) – (11) shows the derivation of the analytical solution used herein. A thermocouple underneath the deposit was used to record the transient deposit temperature during the experiment (T). In order to avoid the latent heat affect, only cooling after the melting point temperature was considered. Acquired experimental data was fitted to estimate the value of h_i which was then used in the numerical simulation model.

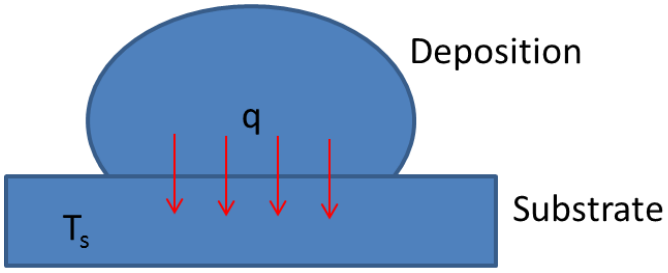

Figure 20: Newtonian cooling model

Heat transfer at interface is given by

$$q = h_i\,(T - T_s) \tag{9}$$

Also, rate of heat loss by the deposition= rate of heat gained by substrate

$$-\rho V C_p \frac{dT}{dt} = h_i A\,(T - T_s) \tag{10}$$

Solving this equation with initial condition (t=0, T=T_0) we get

$$\frac{T - T_s}{T_0 - T_s} = e^{-\frac{h_i A}{\rho V C_p} t} \tag{11}$$

Equation (11) is in non-dimensional form.

where h_i is interfacial heat transfer coefficient, A is interfacial contact area of the deposition and substrate, $\rho\ is$ density, V is volume, C_p is specific heat capacity, To is initial temperature, T_s is substrate temperature and T is temperature of the deposition at any time t.

3.7 Numerical model

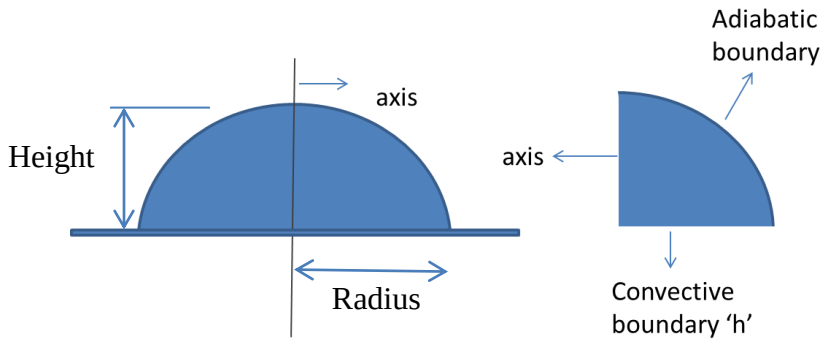

Figure 21: Geometry and boundary condition of numerical model

Figure 21 shows the geometry and boundary condition of the numerical model. To reduce the computational time, 2D axisymmetric model was used to simulate the problem. The radius of the domain for substrate temperatures 150^0C, 175^0C and 195^0C are 2.9 mm, 2.9 mm and 3.5 mm and average heights were 2.9 mm, 2.9 mm and 2 mm respectively. Heat loss is assumed to be only from the base of the deposition defined by convection to the solid substrate and assigned convective boundary condition. Adiabatic boundary condition is assigned on curved surface as heat loss to the surrounding air is considered to be negligible. Fluent was used to carry out the simulation and the energy equation that is solved is given by Equation (12) [20].

$$\frac{\partial}{\partial t}(\rho h) = \nabla.(k\nabla T) + S_h \tag{12}$$

$$h = \int_{T_{ref}}^{T} c_p dT \tag{13}$$

where, h is sensible enthalpy, ρ is density, k is thermal conductivity, S_h is heat source, T is temperature, c_p is specific heat capacity and T_{ref} is reference temperature.

Chapter 4: Results and Discussions

In this section, the bond images, wetting angles, strength of bond from shear test results, heat transfer model using Newton's law of cooling and numerical results are presented. Also, the correlation between bonding images and shear test results as well as theoretical and numerical results has been explored.

4.1 Bond formation

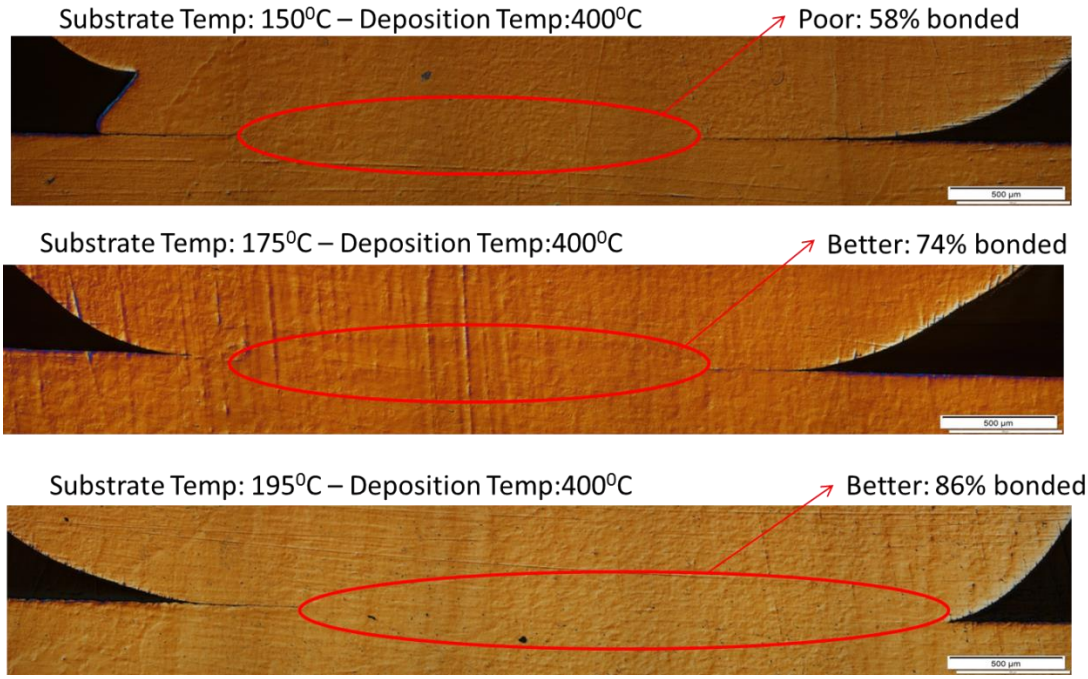

Figure 22: Bonding on air for different substrate temperature

Sample images of interfacial bond at air environment for three different substrate temperatures are shown in Figure 22. The upper curved shape is deposited mass while the bottom one is substrate material. It is observed that no complete bond is observed in any case, however, the bond along the diameter is increased as substrate temperature increased.

Figure 23 shows the sample images of bond at N_2 environment for three different substrate temperatures. At 195^{0}C substrate temperature, complete bond is observed while on others it is

not. The interfacial bond along the diameter has increased compared to the air environment case. Use of inert gas (N_2) is advantageous as it enhances bonding by reducing metal oxidation problem. At 150^0C substrate temperature, we can see that the deposited mass has some void on it which is just above interfacial surface as seen in the picture. These are some issues on AM which are not considered in this research. All sample images of bond formation for air and N_2 environment is in Appendix A.

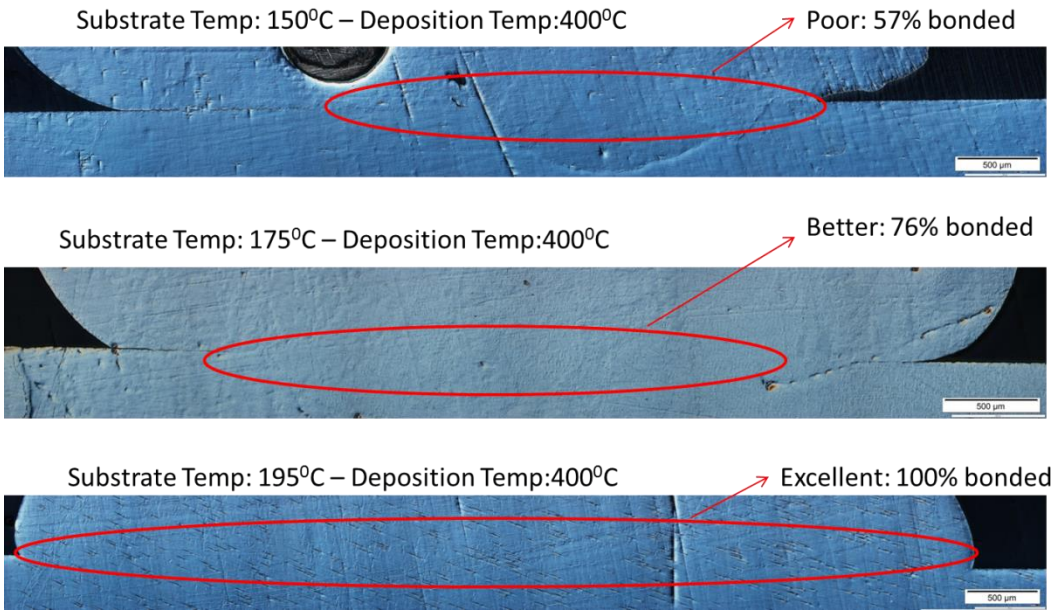

Figure 23: Bonding on N_2 gas for different substrate temperature

Table 2: Comparison of bond on air and N_2 gas

		Air			N_2 gas		
Substrate Temp (^{0}C)	Deposition Temp (^{0}C)	Sample No	% bond along diameter	Average bond	Sample No	% bond along diameter	Average bond
150	400	1	58%	53%	1	50%	60%
		2	65%		2	57%	
		3	38%		3	71%	
175	400	1	54%	66%	1	76%	85%
		2	74%		2	98%	
		3	71%		3	80%	
195	400	1	91%	90%	1	100%	100%
		2	86%		2	100%	
		3	91%		3	100%	

Table 2 shows the comparison between air and N_2 gas and it is seen that the average bond along diameter for same substrate temperature has increased when N_2 gas is used. 100% bond along diameter is observed on N_2 gas for substrate temperature at 195^0C, but not on other substrate temperature as presented on Table 2. From this result, best observed process temperature would be the combination substrate and deposition temperature at 195^0C and 400^0C respectively in N_2 gas environment.

4.2 Wetting Angle

Wetting angle is the angle of contact between the liquid and the solid. When deposition is deposited on substrate, initially it is at liquid phase and thus produces the wetting angle with substrate. It plays a huge role on determining the adhesion of two masses and that's why these results are presented and analyzed in this section. Figure 24 shows the wetting angles for different samples in air environment. Wetting angle has increased from 10^0 to 24^0 as the substrate temperature increases. Angles greater than 90^0 are unusual for computation of wetting angle analysis; one such case is observed in our experimental data where the substrate temperature is 150^0C. It can be seen in Figure 24.

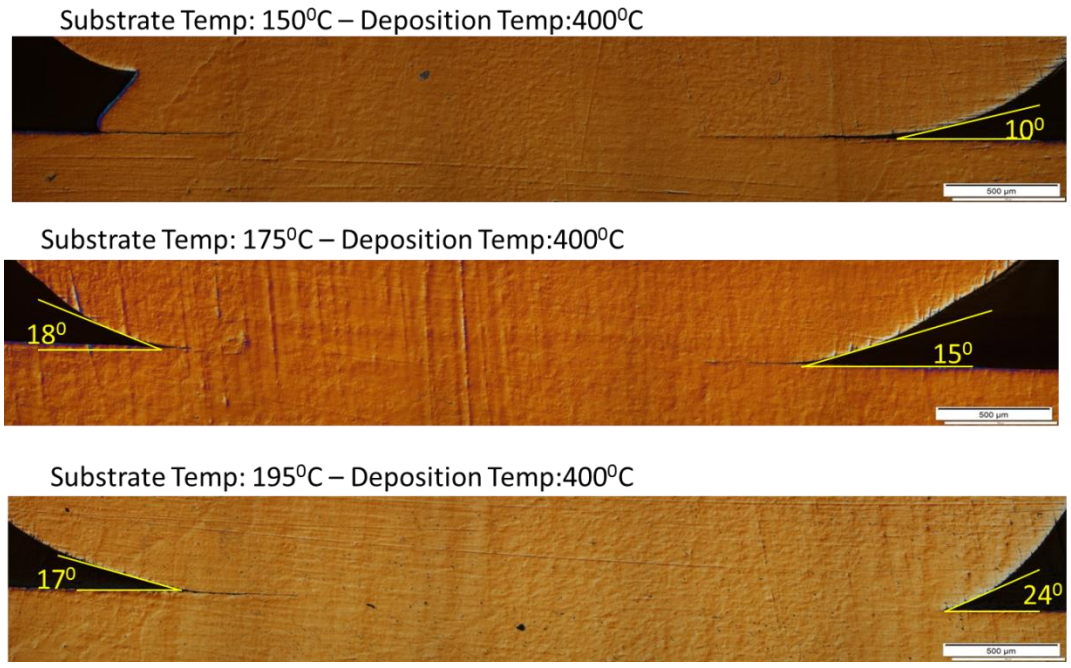

Figure 24: Wetting angle of samples for air

Figure 25 shows the wetting angle of samples in N_2 environment. From the figure it is observed that the wetting angle has significantly increased as we increase the substrate temperature. For substrate temperature 150^0C, 175^0C and 195^0C the wetting angle is around 18^0, 37^0 and 68^0

respectively. If we compare bond images and wetting angles i.e. Figure 21 and Figure 23, it can be noted that higher wetting angle (near 90^0) is necessary for better bonding. Wetting angle near 90^0 is also desirable so that there would be less chance to form voids if successive deposition were made on the substrate.

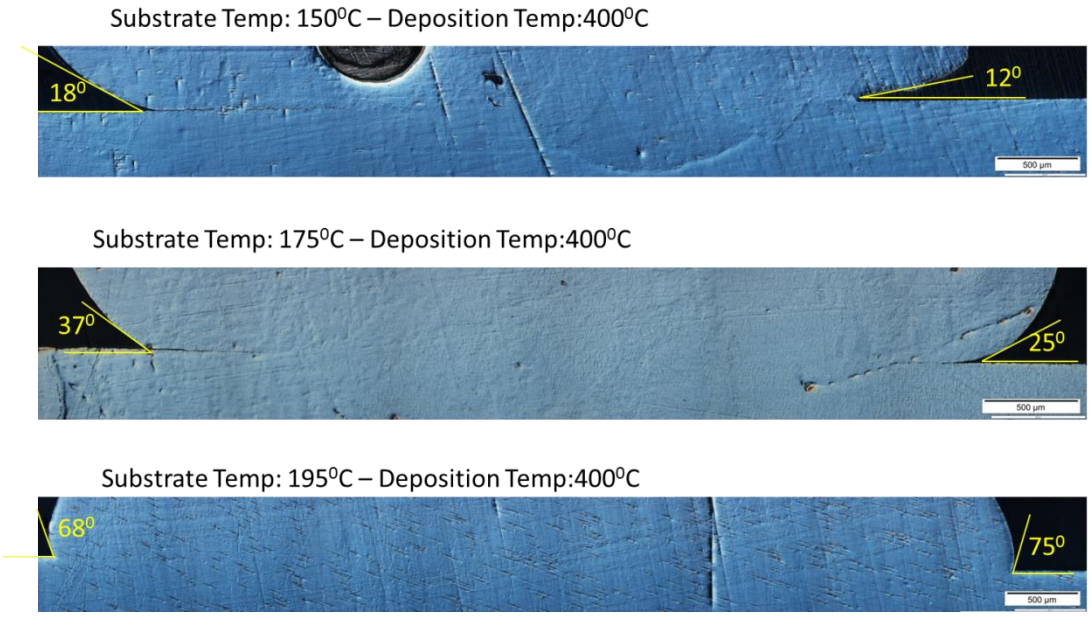

Figure 25: Wetting angle on samples of N_2 gas

Table 3: Comparison of wetting angle on air and N_2 gas

		Air			N_2 gas		
Substrate Temp (^{0}C)	Deposition Temp (^{0}C)	Sample No	Wetting angle (^{0})	Average wetting angle (^{0})	Sample No	wetting angle (^{0})	Average wetting angle (^{0})
150	400	1	10	22.5	1	15	19
		2	30		2	19.5	
		3	28		3	23	
175	400	1	19	19	1	25	29
		2	16.5		2	30	
		3	22		3	31	
195	400	1	18	20	1	44	63
		2	20		2	71.5	
		3	22		3	72	

Table 3 shows the comparison of wetting angle for air and N_2 gas. It is clearly observed that N_2 gas environment has higher wetting angle (except for substrate temperature 150^0C). Air environment has barely or no increase in wetting angle as the substrate temperature is increased, however on N_2 gas the average wet angle has increased from 19^0 to 63^0 as the substrate temperature increased from 150^0C to 195^0C. This result shows that combination of 195^0C substrate temperature and 400^0C deposition temperature is optimum case which has higher wetting angle and helps to make better bond with adjacent deposition reducing chance to form voids due to geometrical shape of deposition.

4.3 Shear test

Shear testing was done to measure the bond strength of the samples. Since the bond images from Figure 20 and Figure 21 only give information about one dimensional interfacial bonding, this test was essential to confirm the bonding on whole interfacial area. Table 4 shows the results of shear test for air and N_2 gas.

Table 4: Shear test result for air and N_2 gas

		Air			N_2 gas		
Substrate Temp (^{0}C)	Deposition Temp (^{0}C)	Sample No	Shear force (N)	Average shear force (N)	Sample No	Shear force (N)	Average shear force (N)
150	400	1	205	190	1	335	357
		2	143		2	312	
		3	218		3	424	
175	400	1	290	280	1	428	428
		2	268		2	460	
		3	281		3	397	
195	40	1	343	320	1	558	562
		2	303		2	562	
		3	312		3	566	

From Table 4, it is observed that for same substrate temperature the shear force was larger with N_2 gas than with air. With both air and N_2 gas, the shear force has increased as the substrate

temperature increases. For N_2 gas the average shear force for 150^0C, 175^0C and 195^0C was 357 N, 428 N and 562 N respectively. For 195^0C substrate temperature, the shear forces for all three samples almost have similar values and the shear force is higher than 150^0C and 175^0C, which shows the proper bonding as expected.

Majority of interest is on stress quantity rather than force. Table 5 shows the shear stress for the N_2 gas case. From metal handbook [21], shear strength of casted tin is 20 MPa, however, for each substrate temperature shear strength of deposition is different and has varied from 16.2 MPa to 28.4 MPa. Theoretically, all cases should have the same shear strength. One reason for this difference in shear strength is due to uncertainty involved in order to find exact interfacial contact area. Here contact area is assumed to be circular shape having diameter equal to contact length observed from metallographic image (Section 4.1) and this assumption might have some errors involved. Maximum possible errors that can be involved in determining contact area for 150^0C, 175^0C and 195^0C case are 50%, 30% and 7% respectively. These errors are determined based on the difference of base area observed from the top surface of deposition (measured from AutoCAD) and assumed circular area from metallographic image. This data is shown in Appendix B. For 195^0C, the shear strength should be close to 20 MPa (from handbook), however the experimental value is 16.2 MPa (20% off). This difference might be because in the difference of shear test method involved in the handbook and this experiment. Another reason for the difference in shear strength could be the microstructure variation of the material because of different substrate temperatures which may have affected the strength of deposition. Likewise for 150^0C, higher shear strength is observed than other cases. One reason could be the uncertainty involved in calculating contact area as described above while another reason could be better mechanical properties when allowed to cool at this substrate temperature.

Table 5: Shear stress for N_2 gas

Substrate Temp(^{0}C)	Deposition Temp(^{0}C)	Average Contact area(m^2)	Stress (MPa)	Contact Area uncertainty error
150	400	1.26e-5	28.4	50%
175	400	1.89e-5	22.7	30%
195	400	3.48e-5	16.2	7%

4.4 Interfacial heat transfer coefficient, h_i

The calculation of h_i involves the following procedures:

1. Recording cooling rate of deposition using thermocouple at the interface of deposition and the substrate after material is deposited on substrate
2. To avoid latent heat effect, cooling after melting point is considered
3. Curve fitting was done by reducing difference in experimental and estimated temperature and h_i is calculated by using other known parameters like mass of deposition, area and specific heat capacity.

Curve fitting samples for substrate temperatures 150^{0}C, 175^{0}C and 195^{0}C are shown in Figure 26, Figure 27 and Figure 28 respectively. This is done only for N_2 gas because only in N_2 gas deposition has made better bond and air environment is not ideal for this manufacturing process.

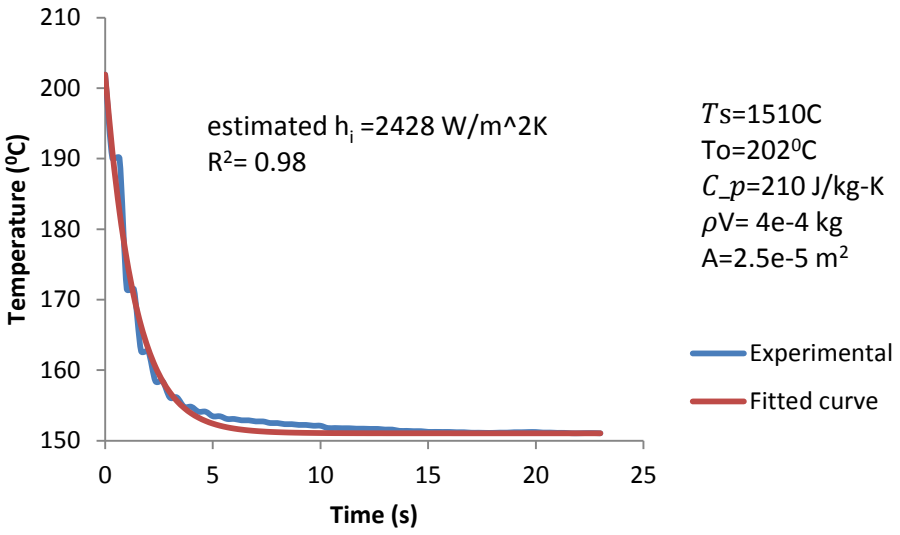

Figure 26: Curve fitting on Substrate temperature 150^0C

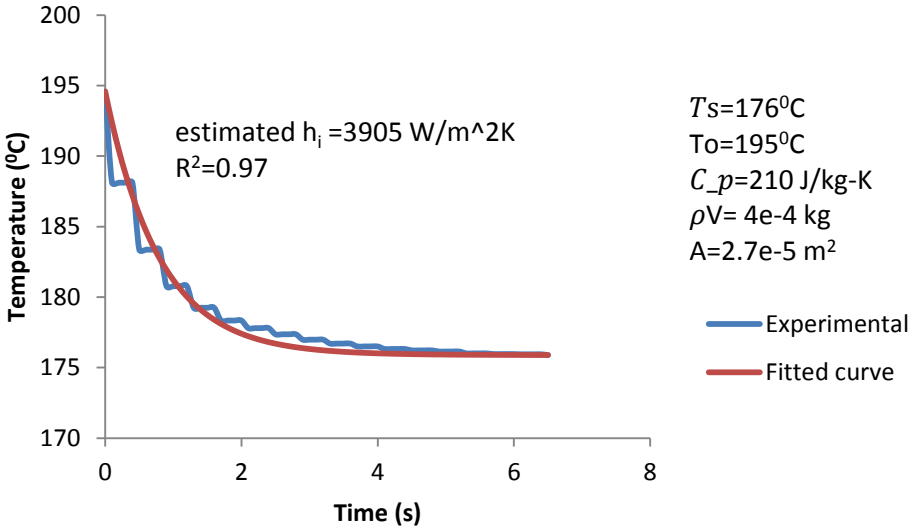

Figure 27: Curve fitting on Substrate temperature 175^0C

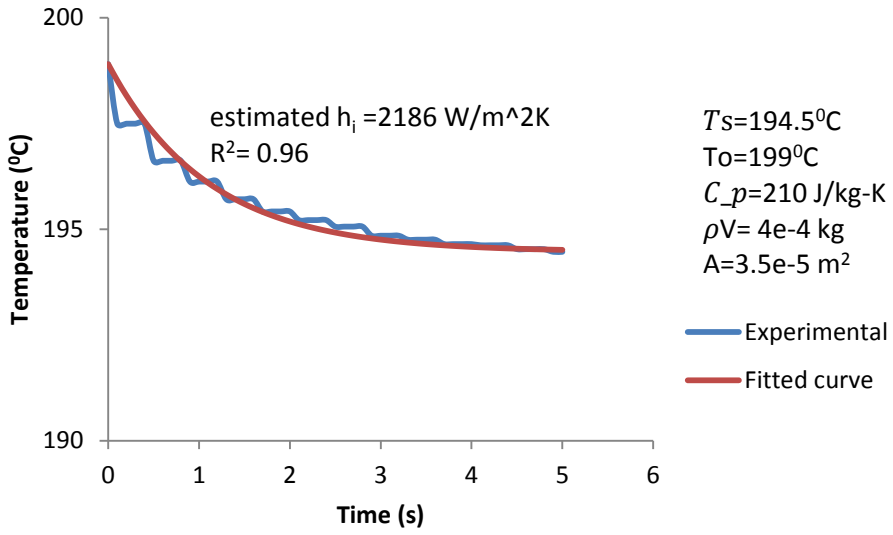

Figure 28: Curve fitting on Substrate temperature 195^0C

Table 6 shows h_i value for all samples and its average for each case. Average h_i value for 150^0C, 175^0C and 195^0C are 2544 W/m^{2}K, 3644 W/m^{2}K and 2530 W/m^{2}K respectively. For 175^0C, h_i is higher and this means higher cooling rate than other cases. One reason for higher h_i could be uncertainty involved in estimating interfacial contact area. Since estimation on h_i depends directly on contact area of deposition, error in calculating h_i is also inevitable as there is some error involved in calculation of contact area (as discussed in Section 4.3). Other reason for higher h_i could be due to influence of substrate temperature that might have changed microstructure thermal properties and enhanced the cooling rate.

Reciprocal of h_i presented in Table 6 would give thermal contact resistance in order of 10^{-4} m^{2}K/W and same order of contact resistance is used in one of the article by Fang et al. [3] for the analysis. In this research these h_i values are used in numerical analysis to produce simulation results and to make comparison with experimental data.

Table 6: h_i value for different case

N_2 gas				
Substrate Temp(0C)	Deposition Temp (0C)	Sample No	h_i (W/m^2K)	Average h_i (W/m^2K)
150	400	1	2428	2544
		2	2423	
		3	2780	
175	400	1	3905	3644
		2	3031	
		3	3995	
195	400	1	2521	2530
		2	2186	
		3	2881	

4.5 Numerical Results

As discussed in above sections, numerical simulation has been carried out to observe the cooling rate using the interfacial heat transfer coefficient from previous section. For numerical solutions, it is essential to evaluate the number of nodes or mesh size to have in a domain so that solution converges. Mesh independent test was carried out using substrate temperature of 175^0C. Mesh of the domain was produced using ICEM CFD and simulation was run on Fluent with an average h_i=3644 W/m^2K, time step of 1e-4 second and absolute energy convergence criteria of 1e-8. Temperature result of every 0.1 second time step was recorded at centroid of the domain to compare with the experimental data.

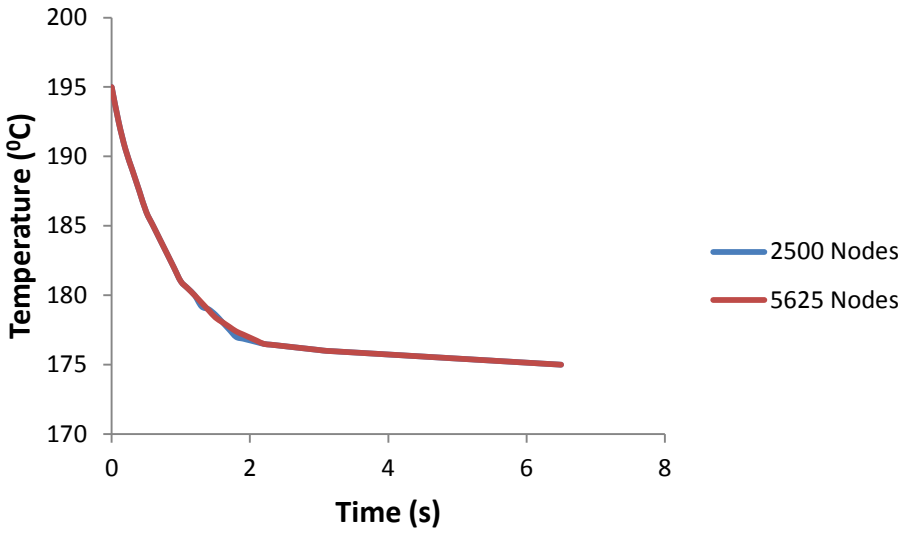

Figure 29: Mesh independent test

Figure 29 shows the mesh independent test where domain with 2500 and 5625 nodes were simulated and it is observed that for both number of nodes the temperature verses time result is the same. So, 2500 nodes case was selected for further analysis. Figure 30 shows the mesh of the domain with 2500 nodes.

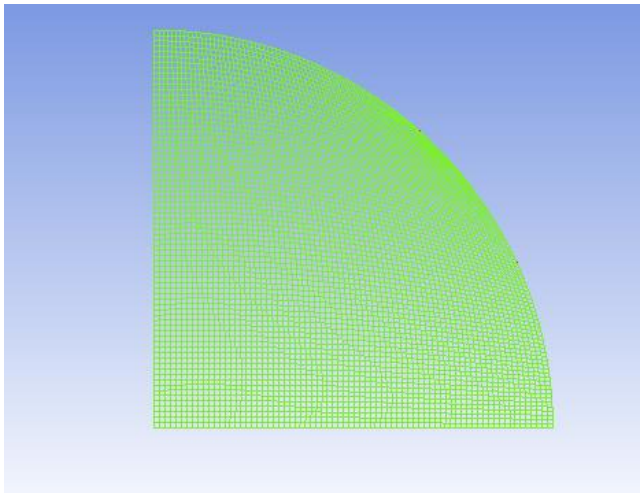

Figure 30: Mesh with 2500 Nodes

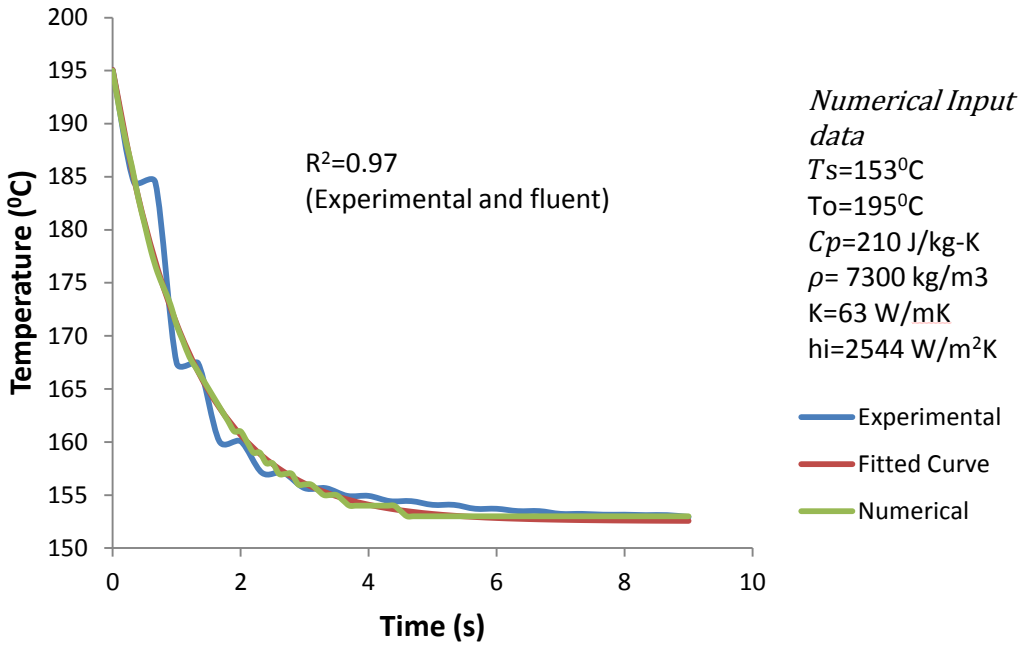

Figure 31: Comparison of Experimental and Numerical results for substrate temperature 150^0C

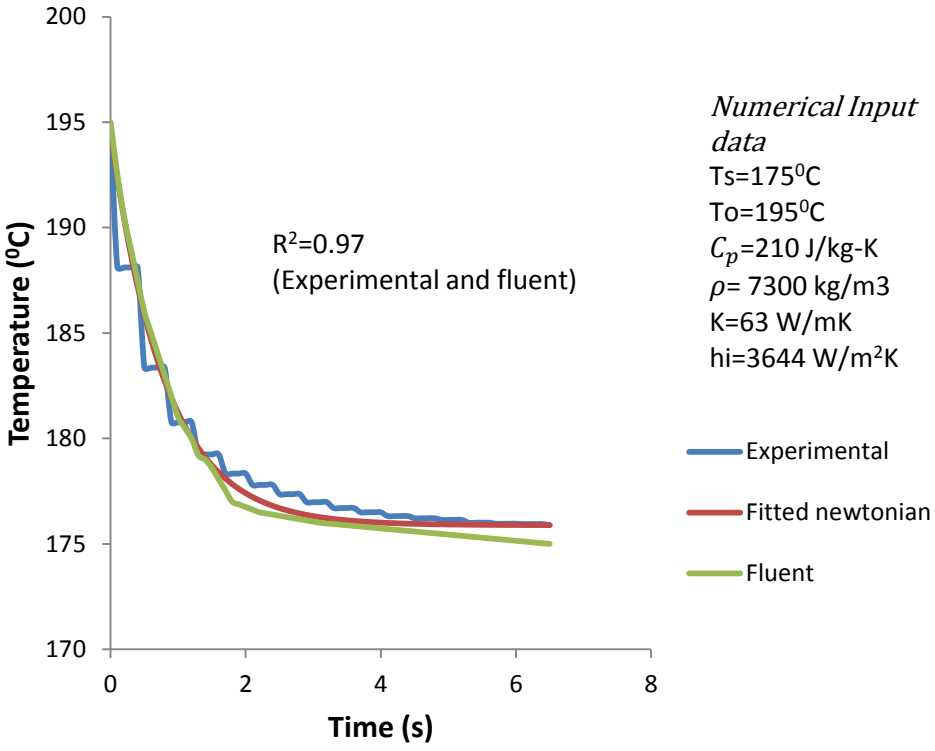

Figure 32: Comparison of Experimental and Numerical results for substrate temperature 175^0C

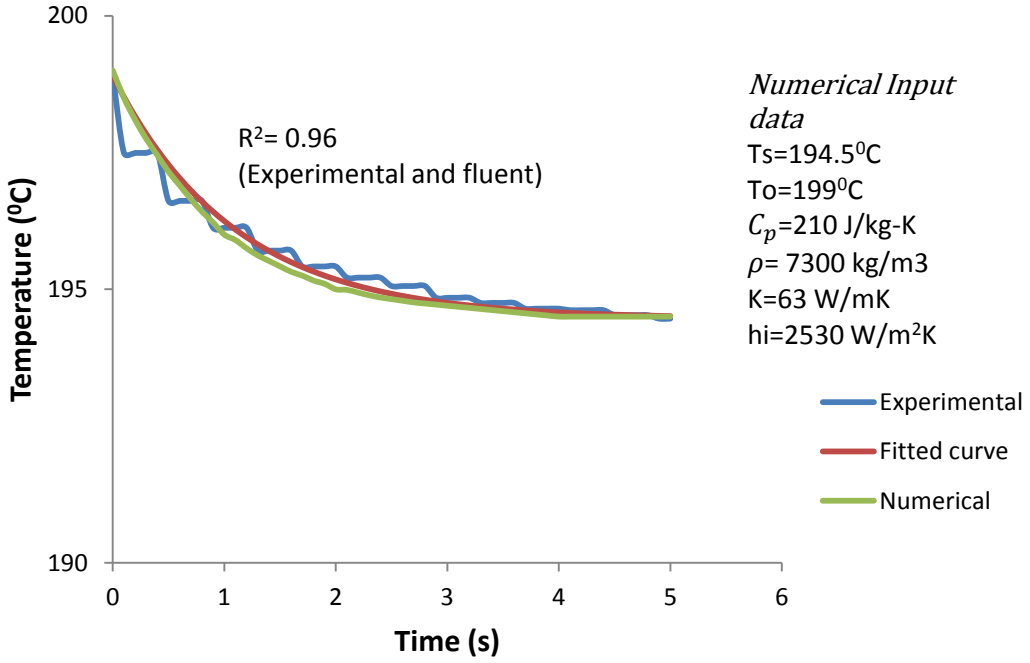

Figure 33: Comparison of Experimental and Numerical results for substrate temperature 195^0C

Figure 31, 32 and 33 shows comparison between experimental and numerical results for substrate temperatures 150^0C, 175^0C and 195^0C respectively. The input parameter for each case is shown in right side of the figure. It is observed that experimental and numerical results match closely for substrate temperatures 150^0C, 175^0C and 195^0C with R^2 values of 0.97, 0.97 and 0.96 respectively. This confirms that interfacial heat transfer coefficient that was estimated in previous section is reasonable and Newton's law of cooling model is appropriate in this case. If multiple deposition were made along line the case could be different, however, h_i value estimated from single deposition still might be helpful in numerical analysis which shows the possibility to extend numerical model for more complex shaped objects.

Chapter 5: Conclusion

The process temperatures (deposition temperature and substrate temperature) and atmosphere are critical to form high-integrity bonds during material jetting additive manufacturing. N_2 gas atmospheres with oxygen levels less than 150 ppm O_2 and a substrate temperature of 195^0C exhibited excellent bonding metallographically and high values of shear strength. In addition, wetting angles of those samples were higher indicating better bonding with substrate throughout the interfacial region. The higher wetting angle (near to 90^0) is also desirable to avoid the possibility of micro-voids and cold lap in two adjacent depositions.

Moreover, the cooling rates of depositions were successfully fit to a Newtonian cooling model and the interfacial heat transfer coefficient h_i estimated as 2530-3644 W/m^{2}K. The agreement of numerical and experimental results shows the possibility of using h_i parameter in numerical model for complex shapes and other alloys.

Finally, it can be said that experiments and investigation using pure tin material were successfully accomplished to study influence of process temperature and environment on interfacial bonding in tin as well as on interfacial heat transfer coefficient h_i during tin deposition. This study has helped to identity a process window to produce more complex shaped objects. It has also demonstrated the use of h_i in simple numerical model and marked its usage for multifaceted numerical model to predict needed process parameters for complex shaped objects.

5.1 Suggestions for future study

Future study on this research could be made on the limitations of this research. The suggestions for future study are listed below:

- Experiments with a range of deposition masses and deposition temperatures are needed to confirm the results presented in this study.
- Effect of temperature on microstructure of material and its strength should be carried out.
- Study on possibility of air entrapment during deposition which is not considered in this research should be examined.
- Use of different materials like aluminum, steel would help to generalize the results.
- Estimated h_i value could provide information about tentative convective heat transfer coefficient; on how to maintain constant substrate temperature while building up vertical columns and walls without changing frequency of deposition. Experiments should be carried out to observe this relationship.
- A more complete multi-physics simulation of the deposition system would include
  - Material jetting from nozzle including fluid dynamics
  - Droplet impact on the substrate
  - Droplet heat transfer and solidification in vertical columns, walls and various 3D shapes

References

[1] M. LaMonica, “Additive Manufacturing,” 2013. [Online]. Available: https://www.technologyreview.com/s/513716/additive-manufacturing/. [Accessed: 20-Jan-2018].

[2] S. A. M. Tofail, E. P. Koumoulos, A. Bandyopadhyay, S. Bose, L. O’Donoghue, and C. Charitidis, “Additive manufacturing: Scientific and technological challenges, market uptake and opportunities,” *Mater. Today*, vol. 21, no. 1, pp. 22–37, 2017.

[3] M. Fang, S. Chandra, and C. B. Park, “Experiments on Remelting and Solidification of Molten Metal Droplets Deposited in Vertical,” vol. 129, pp. 311–318, 2007.

[4] M. Fang, S. Chandra, and C. B. Park, “Heat Transfer During Deposition of Molten Aluminum Alloy Droplets to Build Vertical Columns,” vol. 131, pp. 1–7, 2009.

[5] J. C. Carslaw, H.S., Jaeger, *Conduction of Heat in Solids*. London: Oxford University Press, 1959.

[6] Y. P. Chao, L. H. Qi, H. S. Zuo, J. Luo, X. H. Hou, and H. J. Li, “Remelting and bonding of deposited aluminum alloy droplets under different droplet and substrate temperatures in metal droplet deposition manufacture,” *Int. J. Mach. Tools Manuf.*, vol. 69, pp. 38–47, 2013.

[7] C.-K. Kim, “An analytical solution to heat conduction with a moving heat source,” *J. Mech. Sci. Technol.*, vol. 25, no. 4, pp. 895–899, 2011.

[8] M. Van Elsen, M. Baelmans, P. Mercelis, and J. P. Kruth, “Solutions for modelling moving heat sources in a semi-infinite medium and applications to laser material

processing," *Int. J. Heat Mass Transf.*, vol. 50, no. 23–24, pp. 4872–4882, 2007.

[9] H. Li, P. Wang, L. Qi, H. Zuo, S. Zhong, and X. Hou, "3D numerical simulation of successive deposition of uniform molten Al droplets on a moving substrate and experimental validation," *Comput. Mater. Sci.*, vol. 65, pp. 291–301, 2012.

[10] J. Du and Z. Wei, "Numerical analysis of pileup process in metal microdroplet deposition manufacture," *Int. J. Therm. Sci.*, vol. 96, pp. 35–44, 2015.

[11] S. G. Lambrakos and K. P. Cooper, "A general algorithm for inverse modeling of layer-by-layer liquid-metal deposition," *J. Mater. Eng. Perform.*, vol. 19, no. 3, pp. 314–324, 2010.

[12] D. P. Webb, C. Liu, F. Sarvar, P. P. Conway, and K. Williams, "Adhesion of precision welded lead-free electrical interconnects formed by molten droplet deposition," *Proc. Inst. Mech. Eng. Part B J. Eng. Manuf.*, vol. 221, no. 2, pp. 303–315, 2007.

[13] R. Dhiman and S. Chandra, "Freezing-induced splashing during impact of molten metal droplets with high Weber numbers," *Int. J. Heat Mass Transf.*, vol. 48, no. 25–26, pp. 5625–5638, 2005.

[14] H. Zuo, H. Li, L. Qi, and S. Zhong, "Influence of Interfacial Bonding between Metal Droplets on Tensile Properties of 7075 Aluminum Billets by Additive Manufacturing Technique," *J. Mater. Sci. Technol.*, vol. 32, no. 5, pp. 485–488, 2016.

[15] B. Chang, G. Nave, and S. Jung, "Drop formation from a wettable nozzle," *Commun. Nonlinear Sci. Numer. Simul.*, vol. 17, no. 5, pp. 2045–2051, 2012.

[16] G. Yang and J. A. Ã. Liburdy, "Droplet formation from a pulsed vibrating micro-nozzle,"

vol. 24, pp. 576–588, 2008.

[17] J. Luo, L. Qi, J. Zhou, X. Hou, and H. Li, "Journal of Materials Processing Technology Modeling and characterization of metal droplets generation by using a pneumatic drop-on-demand generator," *J. Mater. Process. Tech.*, vol. 212, no. 3, pp. 718–726, 2012.

[18] J. Luo, L. Qi, Y. Tao, Q. Ma, and C. W. Visser, "Impact-driven ejection of micro metal droplets on-demand," *Int. J. Mach. Tools Manuf.*, vol. 106, pp. 67–74, 2016.

[19] G. H. Poirier, D.R., Geiger, *Transport phenomena in materials processing*. 1994.

[20] *Ansys 14.5 Theory Guide- 5.2.1. Heat Transfer Theory*. .

[21] T. Lyman, *Properties and selection of metals*. Metals Park, Ohio, 1961.

Appendix A: Interfacial bond images

1. Interfacial bond images in air environment

a) 150^0C substrate temperature (three samples)

b) 175^0C substrate temperature (three samples)

c) 195^0C substrate temperature (three samples)

2. Interfacial bond Images in N_2 environment

a) 150^0C substrate temperature (three samples)

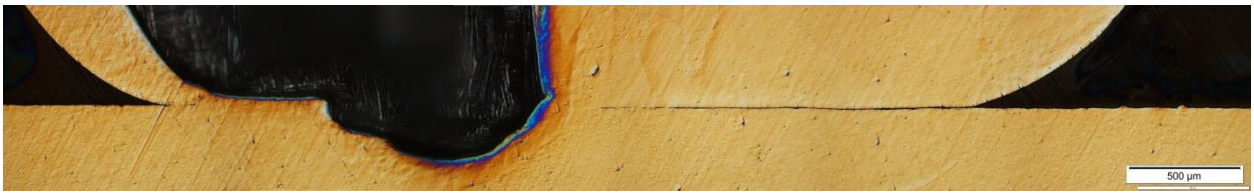

b) 175^0C substrate temperature (three samples)

c) 195^0C substrate temperature (three samples)

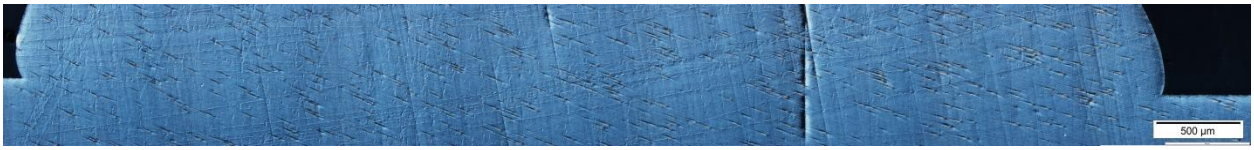
500 µm


500 µm

Appendix B: Difference in interfacial contact area

Substrate Temp(^{0}C)	Deposition Temp(^{0}C)	Average area from metallographic image (assuming circular area) (m^2)	Average area from top surface of deposition (using Autocad) (m^2)	% difference in area
150	400	1.26e-5	2.5e-5	50%
175	400	1.89e-5	2.7e-5	30%
195	400	3.48e-5	3.50e-5	7%